EARTHQUAKE ENGINEERING AND STRUCTURAL DYNAMICS
Earthquake Engng. Struct. Dyn. **28**, 421–441 (1999)

A COUPLING MODEL OF FE–BE–IE–IBE FOR NON-LINEAR LAYERED SOIL–STRUCTURE INTERACTIONS

ZHANG CHUHAN*, CHEN XINFENG AND WANG GUANGLUN
Department of Hydraulic Engineering, Tsinghua University, Beijing, China 100084

SUMMARY

A coupling model of Finite Elements (FEs), Boundary Elements (BEs), Infinite Elements (IEs) and Infinite Boundary Elements (IBEs) is presented for analysis of soil–structure interaction (SSI). The radiation effects of the infinite layered soil are taken into account by FE–IE coupling, while the underlying bed rock half-space is discretized into BE–IBE coupling whereby the non-horizontal bed rock surface can be accounted for. Displacement compatabilities are satisfied for all types of aforementioned elements. The equivalent linear approach is employed for approximation of nonlinearity of the near field soil. This model has some advantages over the current SSI program in considering the bed rock half-space and non-vertical wave incidence from the far field. Examples of verification demonstrate the applicability and accuracy of the method when compared with the FLUSH[2] program. Finally, the effects of the relative modulus ratio E_r/E_s of rock and soil and the incident angles of non-vertical waves on the responses of the structure and the soil are examined. Copyright © 1999 John Wiley & Sons, Ltd.

KEY WORDS: soil–structure interaction; infinite element; infinite boundary element; non-linear layered soil; equivalent linearized method

1. INTRODUCTION

In analysis of dynamic Soil–Structure Interactions (SSI) for important projects such as nuclear structures (power plants and heating structures) built on sites of alluvial deposit, it is of importance that the layered and non-linear properties of the soil can be considered. However, since the dynamic stress–strain behaviour of soils and the factors affecting the behaviour are not easily quantifiable in the current state-of-the-art, the soil is commonly modelled as an equivalent linear viscoelastic medium[1] in SSI analyses for earthquake motion, in which the non-linearities of the soil are accounted for in an approximate manner. This simplified procedure is used in the most popular computer codes of SSI analyses for nuclear structures such as FLUSH[2] and SASSI[3] in the current design practice. Another important consideration in performing the SSI analyses is that the soil model possesses the capability of properly simulating the radiation damping mechanism. The discretization of the layered half-space using the finite element method requires the use of wave-transmitting side boundaries to simulate the lateral radiation effects. Another

* Correspondence to: Zhang Chuhan, Department of Hydraulic Engineering, Tsinghua University, Beijing, China 100084

Contract/grant sponsor: Chinese National Key Projects on Basic Research and Applied Research

CCC 0098–8847/99/040421–21$17·50

Received 13 November 1997
Revised 13 August 1998

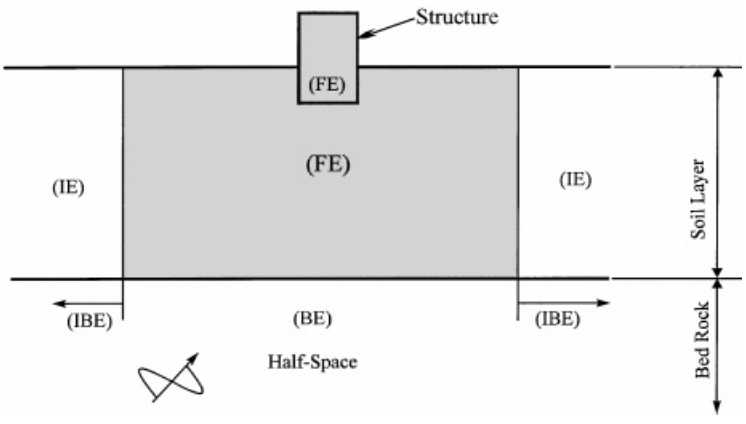

Figure 1. Discretization of soil–structure system

alternative for simulating the radiation effect of infinite soil is simply to use a truncated half-space model in which a sensitivity study must be performed to demonstrate the effects on the impedances of the foundation due to the wave diffractions and reflections by the truncated boundaries are negligible.

In many practical cases for simulating soil foundation system, a 2-D horizontally layered stratum ovelying a rigid base may be assumed such as FLUSH. In this case, the rigid base boundary may be placed at a layer at which the shear wave velocity equals or exceeds 1100 m/s.[4] However, if a deep soft soil or semi-rock is encountered, the rigid base assumption will not be appropriate to describe the radiation effects of the lower boundary or will lead to an expensive cost for discretization of the soil to a great extent of depth. Another limitation of placing the rigid base at the lower boundary is that the inclined wave input can not be performed in the analysis. However, it is important to consider the inclined wave input mechanism which causes rocking and torsional motions of the foundation and may significantly affect the foundation motion and the structural response.

With the above-mentioned considerations, this paper presents a coupling model of Finite Elements (FEs)–Boundary Elements (BEs)–Infinite Elements (IEs) and Infinite Boundary Elements (IBEs) for simulation of soil–structure system for nuclear structures built on a deep soft soil. As shown in Figure 1, FE is employed for discretization of the structure and the near-field soil, in which the linear equivalent viscoelastic assumptions can be applied and the layered characteristics can also be considered. The soil underlying the FE region is a uniform elastic half-space which can be discretized into BEs. The propagating waves from the far-field incident to the half-space surface at varying angles can be applied. To achieve the coupling of the FE region with the lateral layered soil, an improved type of Infinite Element (IE) which is able to transport SV and P waves simultaneously is presented to be installed at the side boundaries. For discretization of the boundary interface between the IE region and the uniform half-space, a type of Infinite Boundary Element (IBE) which is compatible with the IEs is employed. This IBE possesses the same attenuation behaviour of the tractions as the displacements at the far field. Thus, a complete coupling model of FEs–BEs–IEs–IBEs is formed to simulate the linear equivalent and layered soil overlying the elastic half-space. The use of BE–IBE coupling to

discretize the underlying bed rock provides advantage over the half-space solution in dealing with special cases as the bed rock surface is not horizontal or the bed rock medium is not entirely homogeneous. In this case, the discretization method has to be used. On the other hand, if the bed rock surface is horizontal and the medium is homogeneous, to analyse the entire system more efficiently, the substructure technique using analytical solution for half-space may be employed. The entire soil medium is divided into the near and the far fields so that the linear equivalent region of the soil and the computational efforts can be reduced as much as possible. Finally, as a test example, the earthquake response of a structure founded on a soft soil foundation is analysed using the presented model. Verification of accuracy is first achieved by comparing the results with that analysed by FLUSH. To demonstrate the applicability of the presented coupling system, the responses of the structure under the incidence of the waves at different inclined angles are analysed.

2. NUMERICAL MODELLING

2.1. Boundary Elements (BEs) and Infinite Boundary Elements (IBEs) with decaying tractions

The governing equations for elastodynamic problems in the frequency domain can be expressed in terms of boundary integral equations by using the weighted residual procedure and employing the fundamental solutions of the problem as the weighting functions; thus,

$$C_{ij}U_j + \int_\Gamma P^*_{ij}U_j \,\mathrm{d}\Gamma = \int_\Gamma U^*_{ij}P_j \,\mathrm{d}\Gamma \tag{1}$$

where C_{ij} are constants related to the local geometric shape of the boundary at the source point; Γ represents the total boundary (i.e. $\Gamma = \Gamma_u + \Gamma_p$); and U^*_{ij}, P^*_{ij} represent the fundamental solutions which have the form

$$\begin{aligned} U^*_{ij} &= \frac{1}{2\pi\rho c_2^2}[\phi\delta_{ij} - \psi r_{,i}r_{,j}] \\ P^*_{ij} &= \frac{1}{2\pi}\left[\left(\frac{\mathrm{d}\phi}{\mathrm{d}r} - \frac{\psi}{r}\right)\left(\delta_{ij}\frac{\partial r}{\partial n} + r_{,j}n_i\right) - 2\frac{\psi}{r}\left(r_{,i}n_j - 2\frac{\partial r}{\partial n}r_{,i}r_{,j}\right)\right. \\ &\quad \left. - 2\frac{\mathrm{d}\psi}{\mathrm{d}r}\frac{\partial r}{\partial n}r_{,i}r_{,j} + \left(\frac{c_1^2}{c_2^2} - 2\right)\left(\frac{\mathrm{d}\phi}{\mathrm{d}r} - \frac{\mathrm{d}\psi}{\mathrm{d}r} - \frac{\psi}{r}\right)r_{,i}n_j\right] \end{aligned} \tag{2}$$

where δ_{ij} denotes the Kronecker delta and ϕ, ψ are given in terms of Bessel functions by

$$\begin{aligned} \phi &= K_0\left(\frac{\mathrm{i}\omega r}{c_2}\right) + \frac{c_2}{\mathrm{i}\omega r}\left[K_1\left(\frac{\mathrm{i}\omega r}{c_2}\right) - \frac{c_2}{c_1}K_1\left(\frac{\mathrm{i}\omega r}{c_1}\right)\right] \\ \psi &= K_2\left(\frac{\mathrm{i}\omega r}{c_2}\right) - \frac{c_2^2}{c_1^2}K_2\left(\frac{\mathrm{i}\omega r}{c_1}\right) \end{aligned} \tag{3}$$

in which K_m are modified Bessel functions of the second kind of order m; r represents the distance between the source and field points; and n_i is the direction cosine in direction i at the field point.

By discretizing the boundaries into elements and using interpolation functions to describe the displacement and traction, the following set of linear equations is obtained:

$$HU = GP \tag{4}$$

where

$$H = H' + C \tag{5}$$

and in which U and P are the nodal displacements and the traction; C is the constant matrix constituted from C_{ij}; and H' and G are coefficient matrices which are assembled from individual element matrices given by

$$\begin{aligned} H'^{e} &= \int_{-1}^{+1} [P^*][N]|J|\,\mathrm{d}\xi \\ G^{e} &= \int_{-1}^{+1} [U^*][N]|J|\,\mathrm{d}\xi \end{aligned} \tag{6}$$

where $[P^*]$ and $[U^*]$ are matrices formed from the fundamental solutions; $[N]$ represents the interpolation shape function matrix; ξ is the natural coordinate, and $|J|$ is the Jacobian determinant for co-ordinate transformation.

The integration singularity caused by functions U_{ij}^* and P_{ij}^* can be treated by dividing these into static counterparts plus additional terms as follows[5]:

$$\begin{aligned} U_{ij}^* &= \bar{U}_{ij}^* + \Delta U_{ij}^* \\ P_{ij}^* &= \bar{P}_{ij}^* + \Delta P_{ij}^* \end{aligned} \tag{7}$$

in which $\bar{U}_{ij}^*$ and $\bar{P}_{ij}^*$ are the fundamental solutions for static problems with singularity of order $\ln r$ and $1/r$, respectively; and ΔU_{ij}^*, ΔP_{ij}^* are additional terms with no singularity in the integration. Hence, the technique employed in static problems is also suitable for overcoming singularity in dynamic problems.

Starting from the concepts of boundary elements and infinite elements the idea of IBE is a combination of BEs and IEs.[5] It was presented by Zhang and Song[6,7] and later was extended to model the far field of arch dam canyons by Zhang and Jin.[8] This paper extends the function of IBE to discretize the interface between the bottom layers on the two sides and the underlying half-space, in which a decaying variation of displacements and tractions from the near to the far field needs to be simulated.

As shown in Figure 2, a two node element with decaying displacements and tractions is developed and is mapped from the global into the natural co-ordinate system using the following mapping relationship:

$$r = r_1 + \frac{1+\xi}{2}\lambda_s + (m-1)\lambda_s, \quad m = 1, 2, 3, \ldots \tag{8}$$

where r and ξ are the global and natural co-ordinate, respectively; λ_s is the wavelength for s component; m denotes the number of wavelength to be integrated; r_1 is the distance between node 1 and 2 which is also defined as the distance from the origin to the node 1.

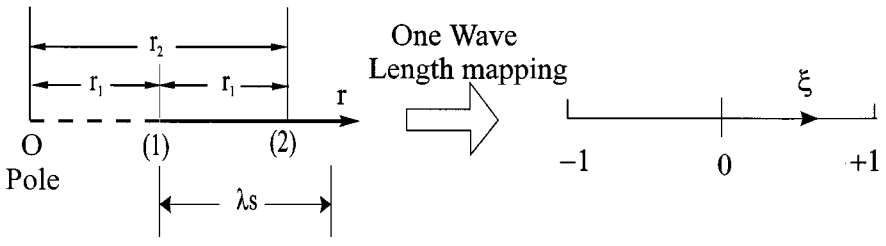

Figure 2. Mapping relationship of the IBE

By using the mapping function given in equation (8), for $m = 1$, the node 1 with $r = r_1$ is mapped into $\xi = -1$ while the point $r = r_1 + \lambda_s$ is mapped into $\xi = 1$. Thus, for $m = 1, 2, 3, \ldots$, the global co-ordinate r is completely transformed into the natural co-ordinate ξ from one wavelength to another until $r \to \infty$.

Since the asymptotic behaviours of the fundamental solutions U_{ij}^* and P_{ij}^* are of following forms:

$$U_{ij}^* \propto 0\left(\frac{1}{\sqrt{r}}e^{-ikr}\right)$$
$$P_{ij}^* \propto 0\left(\frac{1}{\sqrt{r}}e^{-ikr}\right) \tag{9}$$

the shape functions of the displacements of the IBE with two nodes can be assumed as

$$U = \frac{1}{\sqrt{r}}(a_u e^{-ik_P r} + b_u e^{-ik_S r}) = \sum_{i=1}^{2} \bar{N}_i(r) U_i \tag{10}$$

where k_P, k_S are wave numbers of P and S waves respectively; a_u, b_u are coefficients; $\bar{N}_i$ are displacement shape functions.

From equation (10) and the nodal displacement of the element, the displacement shape function $\bar{N}_i$ can be derived as

$$\bar{N}_1(r) = \frac{\sqrt{r_1}}{\sqrt{r}\Delta}(e^{-ik_S r_2}e^{-ik_P r} - e^{-ik_P r_2}e^{-ik_S r})$$
$$\bar{N}_2(r) = \frac{\sqrt{r}}{\sqrt{r}\Delta}(-e^{-ik_S r_1}e^{-ik_P r} + e^{-ik_P r_1}e^{-ik_S r}) \tag{11}$$

where Δ is the determinant

$$\Delta = \begin{vmatrix} e^{-ik_P r_1} & e^{-ik_S r_1} \\ e^{-ik_P r_2} & e^{-ik_S r_2} \end{vmatrix} \tag{12}$$

The same shape functions as equation (11) are also used for traction approximation since both the displacements and the tractions have the same form of asymptotic behaviour as shown

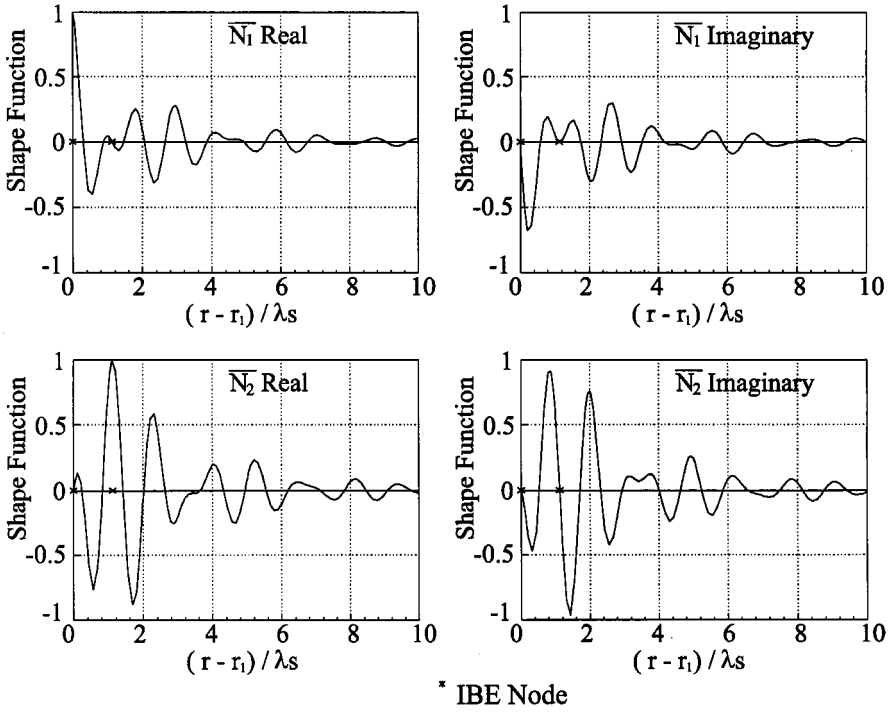

Figure 3. Shape functions of the IBE

in equation (9), thus

$$P = \sum_{i=1}^{2} \bar{N}_i(r) P_i \tag{13}$$

The shape functions $\bar{N}_i(r)$ are plotted in Figure 3 from which the decaying trigonometric characteristics of the functions are evident.

To obtain the contributions of the infinite boundary elements, the integrations $\int_{r_e} P^* \bar{N}\, \mathrm{d}r$ and $\int_{r_e} U^* \bar{N}\, \mathrm{d}r$ need to be calculated. For computation of these integrations, the infinite boundary elements need to be divided into several sections each of which contains one wavelength. The integrations are carried out from one wavelength to another starting from the near to the far field, i.e.

$$\int_{r_e} P^* \bar{N}\, \mathrm{d}r = \frac{\lambda s}{2} \sum_{m=1}^{Ns} \sum_{i=1}^{N\xi} P^*(\xi_i) \bar{N}(\xi_i) W_i \tag{14}$$

where N_s denotes the number of wavelength needed to be calculated for convergence; N_ξ is the number of Gaussian integration points in one wavelength; ξ_i and W_i are co-ordinates of the Gaussian point and the corresponding weighting coefficients; note that $\mathrm{d}r = (\lambda s/2)\,\mathrm{d}\xi$ as shown in equation (8). By setting a predetermined tolerance, either use of λ_s or λ_p (p wavelength) does not affect the final convergence and accuracy of the results.

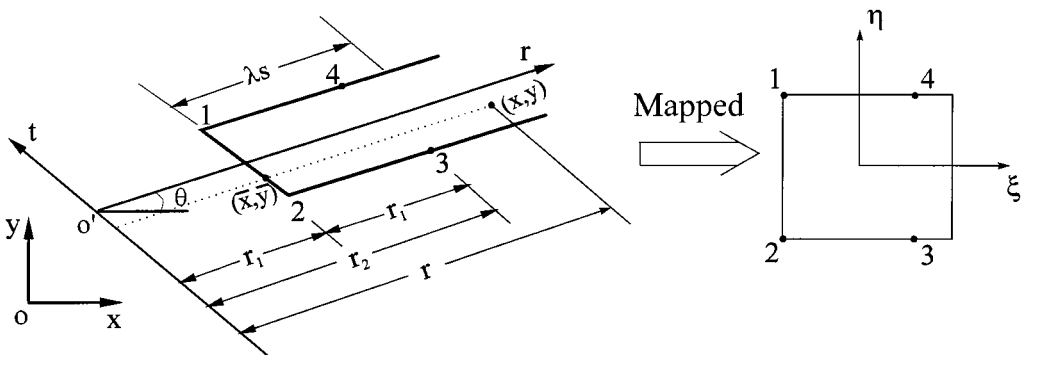

Figure 4. Mapping relationship of the IE

Similar treatment is applied to the integration $\int_{r_e} U^* \bar{N}\, \mathrm{d}r$. In practical calculation, integration of six wavelengths is sufficient for engineering accuracy. The above integrations are assembled into the coefficient matrices H and G of the normal boundary element system in equation (4). Thus, the half-space surface with decaying tractions can be simulated by BE–IBE coupling system.

2.2. *Infinite Elements (IEs) with multi-wave numbers*

The concept of infinite elements was first presented by Ungless[9] and Bettess,[10] and subsequently studied by a number of researchers.[11–13] Zhang and Zhao[14,15] studied the infinite elements comprehensively for simulation of infinite foundations. A review of this element was given by Zhang and Wang.[16] Herein, an improved type of the IE in compatible with the IBE described above is presented for modelling of the layered soil beyond the near field. The innovative point is that it allows P and SV waves to propagate within the element.

In order to have a displacement compatibility with the IBEs, the mapping relationship of the IE is depicted in Figure 4, where r, t and ξ, η represent the local and natural co-ordinate system, respectively, whereas x, y represent the original global co-ordinate system. The same mapping functions for IBEs in equation (8) are again used for IE in infinite r direction and that the linear interpolation is employed for finite t direction, i.e.

$$\begin{aligned} t &= \frac{1+\eta}{2} t_1 + \frac{1-\eta}{2} t_2 \\ r &= r_1 + \frac{1+\xi}{2} \lambda_s + (m-1)\lambda_s \end{aligned} \tag{15}$$

in which λ_s and m have the same definition as in equation (8).

Considering the relationship between global co-ordinate system and local co-ordinate r, t system:

$$\begin{aligned} x &= \bar{x} + (r - r_1)\cos\theta \\ y &= \bar{y} + (r - r_1)\sin\theta \end{aligned} \tag{16}$$

where $\bar{x}$, $\bar{y}$ are co-ordinates of a reference point which is the intersection of the finite boundary of the element and the line which is parallel with the r-axis and passing through the field point (x, y); θ denotes the angle between r- and x-axis. From equations (15) and (16) the mapping relationship between the global co-ordinate x, y system and the natural co-ordinate ξ, η system can be derived as

$$\begin{aligned} x &= \left(\frac{1+\eta}{2}x_1 + \frac{1-\eta}{2}x_2\right) + \left[\frac{1+\xi}{2}\lambda_2 + (m-1)\lambda_s\right]\cos\theta \\ y &= \left(\frac{1+\eta}{2}y_1 + \frac{1-\eta}{2}y_2\right) + \left[\frac{1+\xi}{2}\lambda_2 + (m-1)\lambda_s\right]\sin\theta \end{aligned} \tag{17}$$

where x_1, y_1, and x_2, y_2 are global co-ordinates of points 1 and 2, respectively.

With the mapping functions of equation (17), the global x, y co-ordinates can be completely mapped into the natural ξ, η co-ordinate system from one wavelength to another when $m = 1, 2, 3, \ldots$.

The same decaying patterns of the displacement shape functions $\bar{N}_i(r)$ $(i = 1, 2)$ as equation (11) are used for attenuation in r direction of infinite elements and the element shape functions have the form

$$\begin{aligned} N_1 &= \frac{1+\eta}{2}\bar{N}_1(r), \quad N_2 = \frac{1-\eta}{2}\bar{N}_1(r) \\ N_3 &= \frac{1-\eta}{2}\bar{N}_2(r), \quad N_4 = \frac{1+\eta}{2}\bar{N}_2(r) \end{aligned} \tag{18}$$

Thus, the conditions of displacement compatibility between the IBEs and IEs are assured. Evidently, from equations (11) and (18) $\bar{N}_i(r)$ possess both k_p and k_s wave numbers, thus allowing the infinite element to transport s and p waves simultaneously. Since the asymptotic behaviours of N_i and $\partial N_i/\partial r$ when $r \to \infty$ have the following forms:

$$\begin{aligned} N_i &\propto \left(\frac{1}{\sqrt{r}}\,\mathrm{e}^{-\mathrm{i}kr}\right) \\ \frac{\partial N_i}{\partial r} &\propto \left(\frac{1}{\sqrt{r}}\,\mathrm{e}^{-\mathrm{i}kr}\right) \end{aligned} \qquad (i = 1, 2, 3, 4) \tag{19}$$

the generalized integration for stiffness and mass matrices $[K]^e$ and $[M]^e$ of the infinite elements are convergent when $r \to \infty$.

The integration for obtaining $[K]^e$ and $[M]^e$ for the infinite elements is performed and executed from one wavelength to another as done for infinite boundary elements. Assembling the contributions of IEs to the corresponding stiffness and mass matrices of the FE, the coupling system of FE and IE can be constructed.

2.3. FE–BE–IE–IBE coupling for modelling soil–structure interaction

The schematic system shown in Figure 5(a) is a typical soil–structure interaction problem. The seismic input waves are propagating upward from the bed rock half-space underneath the soil

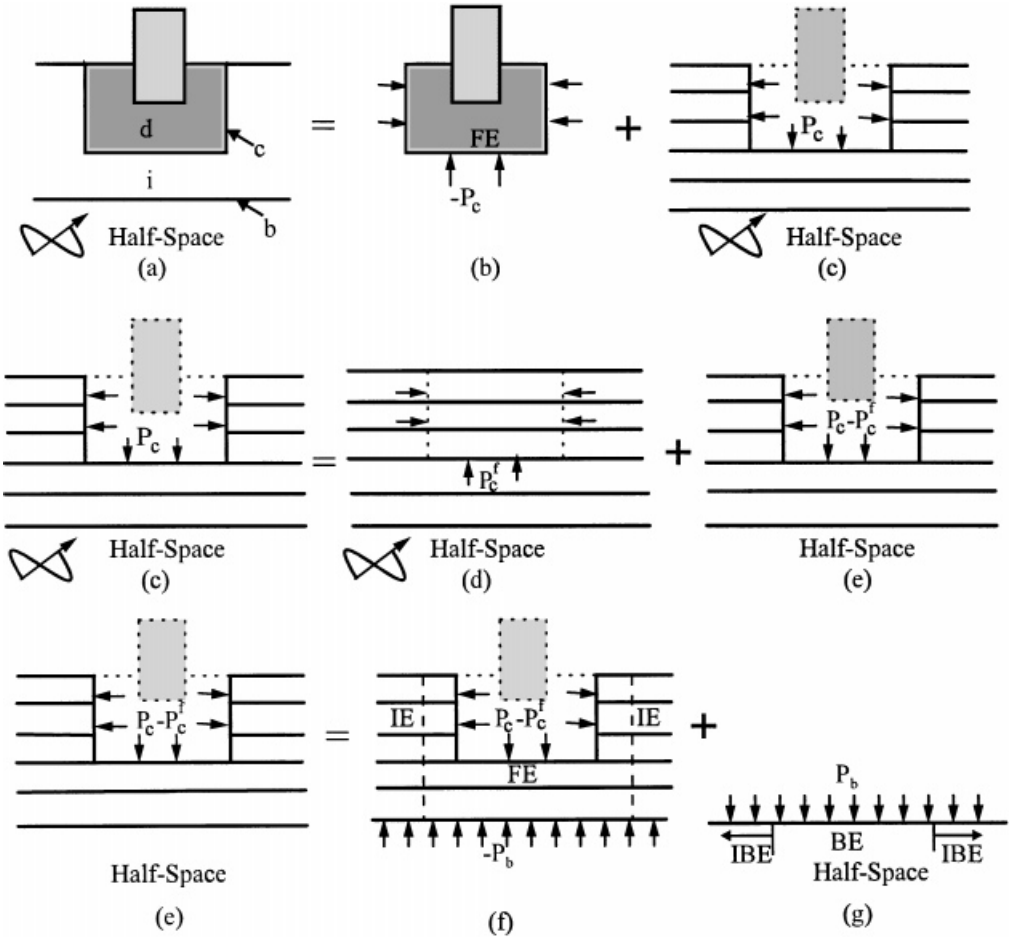

Figure 5. Schematic representation of SSI

layers. The time histories of these waves may be obtained by deconvolution technique after the design ground motion is specified as free-surface motion on the top of competent foundation material or the outcrop at the site. The structure and the near-field soil shown in Figure 5(b) are discretized into finite elements of which the linear equivalent model can be applied to the latter. A transition ring of finite elements between the two vertical dash lines of Figure 5(f) may also be set up for better connection for the near-field FE region with the far-field layers and with the half-space. Beyond the transition zone the soil is discretized into IEs on two sides and into BEs–IBEs on the half-space interface. Thus, the whole system under wave propagation shown in Figure 5(a) can be divided into two subdomains, i.e. the structure and the near-field soil with interaction traction $-P_c$ (Figure 5(b)) and remainder of the layers and the half-space under the wave incidence and the traction P_C on the near-field boundaries (Figure 5(c)). Again, the system of Figure 5(c) can be redivided into the incident wave field of horizontal layers (Figure 5(d)) and the

corresponding scattering field depicted in Figure 5(e), the latter may be redivided into two subdomains as shown in Figures 5(f) and 5(g).

The dynamic equation for harmonic problems can be written as

$$SU = F \tag{20}$$

where U represents the nodal displacement amplitudes; F is the amplitudes of harmonic loads; and S denotes the dynamic stiffness matrix.

First, as shown in Figures 5(a) and 5(b) the degrees of freedom of the structure and near-field soil are divided into interior domain d and the common boundary c, thus equation (20) can be partitioned as follows:

$$\begin{bmatrix} S_{dd} & S_{dc} \\ S_{cd} & S_{cc} \end{bmatrix} \begin{Bmatrix} U_d \\ U_c \end{Bmatrix} = \begin{Bmatrix} 0 \\ F_c \end{Bmatrix} \tag{21}$$

in which the nodal forces F_c are transformed from boundary traction P_c, i.e. $F_c = -M_p P_c$ in which M_p is the transformation matrix constructed from the interpolation shape functions.

Secondly, the transition ring and the remainder of the infinite soil layers can be divided based on degrees of freedom associated with c, i and b shown in Figures 5(a) and 5(f) and the dynamic equation of this subregion can be partitioned as

$$\begin{bmatrix} S_{cc} & S_{ci} & 0 \\ S_{ic} & S_{ii} & S_{ib} \\ 0 & S_{bi} & S_{bb} \end{bmatrix} \begin{Bmatrix} U_c^{\mathrm{s}} \\ U_i^{\mathrm{s}} \\ U_b^{\mathrm{s}} \end{Bmatrix} = \begin{Bmatrix} -F_c + F_c^{\mathrm{f}} \\ 0 \\ F_b \end{Bmatrix} \tag{22}$$

where superscripts s and f represent the scattering and the free fields; again, $F_c^{\mathrm{f}} = -M_p P_c^{\mathrm{f}}$ and $F_b = -M'_p P_b$, in which M'_p is the transformation matrix of the shape functions of the half-space boundary.

Third, for the domain of half-space with traction P_b shown in Figure 5(g) the formulations of coupling BEs and IBEs are derived as

$$H_b U_b^{\mathrm{s}} = G_b P_b \tag{23}$$

where H_b and G_b are the coefficient matrices derived from the half-space boundaries by coupling BEs and IBEs. Premultiplying equation (23) by $M'_p G_b^{-1}$ yields

$$S' U_b^{\mathrm{s}} = -F_b \tag{24}$$

where

$$S' = M'_p G_b^{-1} H_b \tag{25}$$

Substituting equation (24) into equation (22) and combining U_b^{s} and U_i^{s} as $U_{\mathrm{e}}^{\mathrm{s}}$

$$\begin{bmatrix} S_{cc} & S_{ce} \\ S_{ec} & S_{ee} \end{bmatrix} \begin{Bmatrix} U_c^{\mathrm{s}} \\ U_{\mathrm{e}}^{\mathrm{s}} \end{Bmatrix} = \begin{Bmatrix} -F_c + F_c^{\mathrm{f}} \\ 0 \end{Bmatrix} \tag{26}$$

or

$$S'_{cc} U_c^{\mathrm{s}} = -F_c + F_c^{\mathrm{f}} \tag{27}$$

in which

$$S'_{cc} = S_{cc} - S_{ce}S_{ee}^{-1}S_{ec} \tag{28}$$

and noting that

$$U_c = U_c^s + U_c^f \tag{29}$$

Combining equations (21), (27) and (29) provides the equations for a complete system in the form

$$\begin{bmatrix} S_{dd} & S_{dc} \\ S_{cd} & S_{cc} + S'_{cc} \end{bmatrix} \begin{Bmatrix} U_d \\ U_c^s \end{Bmatrix} = \begin{Bmatrix} -S_{dc}U_c^f \\ -M_pP_c^f - S_{cc}U_c^f \end{Bmatrix} \tag{30}$$

where U_c^f and P_c^f are the free field displacements and tractions of the layered half-space shown in Figure 5(d) of which the solutions are available in Reference 17.

By solving equation (30), the displacement fields $[U_d\ U_c^s]^T$ can be obtained. Then, using the relationship of equation (29) the total responses of displacement fields of the structure and the near-field soil $[U_d\ U_c]^T$ are solved.

2.4. *Equivalent linear model*[1] *for near-field soil*

As an approximation of a truly non-linear soil, the equivalent linear model[1] replaces the non-linear constitutive relation with a shear modulus and material damping values selected to be compatible with the so-called effective shear strains induced during the earthquake motion. The parameters required for the analysis are low strain shear modulus and Poisson's ratio, material damping values, and their variations with strain level.

The effective shear strain γ_{eff} is defined as

$$\gamma_{\text{eff}} = 0{\cdot}65 \max_t |\gamma_{\max}| \tag{31}$$

in which $\max_t$ denotes the maximum value for time history; $|\gamma_{\max}|$ represents the strain history in the plane of maximum shear strain; 0·65 is an empirical coefficient.

The root mean square method is employed to obtain the maximum shear strain $\max_t |\gamma_{\max}|$ in the frequency domain and it can be approximately expressed as

$$\max_t |\gamma_{\max}| \approx C\,\text{RMS}(\gamma_{\max}) \tag{32}$$

where $\text{RMS}(\gamma_{\max})$ is the root mean square of $\gamma_{\max}$ and C denotes a coefficient of the shear strain ratio which may be assumed using the same definition of the ratio for the ground motion $\ddot{y}(t)$, i.e.

$$C = \max_t |\ddot{y}(t)| / \text{RMS}(\ddot{y}) \tag{33}$$

where $\max_t |\ddot{y}(t)|$ is the peak acceleration of the control motion of the design earthquake; $\text{RMS}\,\ddot{y}(t)$ is the root mean square of $\ddot{y}(t)$. Combining equations (31)–(33) provides the effective shear strains in the form

$$\gamma_{\text{eff}} \approx 0{\cdot}65 \frac{\text{RMS}(\gamma_{\max})}{\text{RMS}(\ddot{y})} \max_t |\ddot{y}(t)| \tag{34}$$

The procedure of the linear equivalent method includes the following steps: First, using the low strain shear modulus G_0 and damping ratio ξ_0 (i.e. initial values) the amplitudes of linear strains ε_x, ε_y, γ_{xy} for each frequency component ω_s and the root mean squares of the amplitudes of the shear strains $\mathrm{RMS}(\gamma_{\max})$ can be obtained. Secondly, using the current values of $\mathrm{RMS}(\gamma_{\max})$ the first approximation of γ_{eff} for each element can be obtained from equation (34); Third, using the current values of γ_{eff} and consulting the strain-compatible soil properties, new values of shear modulus $G_1(\gamma_{\mathrm{eff}})$ and the damping ratios $\xi_1(\gamma_{\mathrm{eff}})$ for each element can be found from the variation curves of $G(\gamma)$ and $\xi(\gamma)$. These new values of $G_1(\gamma_{\mathrm{eff}})$ and $\xi_1(\gamma_{\mathrm{eff}})$ are subsequently used as new parameters for further iteration. Repeat the same process until the errors between $G_{i+1}(\gamma_{\mathrm{eff}})$ and $G_i(\gamma_{\mathrm{eff}})$, and $\xi_{i+1}(\gamma_{\mathrm{eff}})$ and $\xi_i(\gamma_{\mathrm{eff}})$ are within a predetermined tolerance. Thus, the values $G_{i+1}(\gamma_{\mathrm{eff}})$ and $\xi_{i+1}(\gamma_{\mathrm{eff}})$ are selected to be the equivalent linear modulus and damping ratios for non-linear soil. The corresponding response of the structure or the free field motions can be obtained. Two important points are noteworthy in practical computation.

(1) After a preliminary convergence of the iteration for the near-field soil, the material parameters G and ξ of the finite elements for transition zone and the infinite elements for the far field are changed accordingly to be the same as that of the neighbouring finite elements of the near field. Additional iterations are needed for final convergence.
(2) The free field solution of the layers overlying the half-space U_c^{f} and P_c^{f} in Figure 5(d) is also repeated accordingly using the updated values of the parameters.

3. NUMERICAL VERIFICATION AND APPLICATION

3.1. Free-field response of a soil layer overlying on elastic half-space

The example shown in Figure 6 is a linear soil layer with linear variation of increasing stiffness with depth. The velocity of S wave at the bottom of the layer is as five times as that of the surface. Underlying is a bed rock half-space with elastic property. The same problem was solved analytically by Wolf.[17] The following non-dimensional parameters are defined:

$$\bar{C}_{\mathrm{s}} = \frac{C_{\mathrm{S}}^{\mathrm{R}}}{C_{\mathrm{S}}^{\mathrm{L}}}, \quad \bar{\rho} = \frac{\rho^{\mathrm{R}}}{\rho^{\mathrm{L}}}, \quad a_0 = \frac{\omega d}{C_{\mathrm{S}}^{\mathrm{L}}} \tag{35}$$

in which $C_{\mathrm{S}}^{\mathrm{R}}$ and $C_{\mathrm{S}}^{\mathrm{L}}$ are S wave velocities for the bed rock and soil layer (average), respectively; ρ^{R} and ρ^{L} are mass density, respectively; $\bar{C}_{\mathrm{S}}$, $\bar{\rho}$ are ratios of velocity and mass density, respectively; a_0 is the non-dimensional frequency; d is the depth of the soil layer. Also, the average velocity of the soil layer is defined as

$$C_{\mathrm{S}}^{\mathrm{L}} = \frac{\mathrm{d}}{\int_0^d \mathrm{d}z/C_{\mathrm{s}}(z)} \tag{36}$$

In this analysis, $\bar{C}_{\mathrm{s}} = 2{\cdot}012$; $\bar{\rho} = 1{\cdot}0$; $\eta^{\mathrm{R}} = \eta^{\mathrm{L}} = 0{\cdot}1$; $\upsilon^{\mathrm{R}} = \upsilon^{\mathrm{L}} = 0{\cdot}33$ are assumed, in which η and υ are viscous damping and Poisson's ratio, respectively.

As shown in Figure 6(a), the propagating waves with amplitudes $A_{\mathrm{P}}^{\mathrm{R}}$ and $A_{\mathrm{SV}}^{\mathrm{R}}$ represent the incident P and SV waves from rock with incident angles of $\psi_{\mathrm{P}}^{\mathrm{R}}$ and $\psi_{\mathrm{SV}}^{\mathrm{R}}$, respectively; u_{t} and v_{t} are horizontal and vertical displacement responses on the top of the soil layer. The meanings of other symbols are described in Figure 6(a).

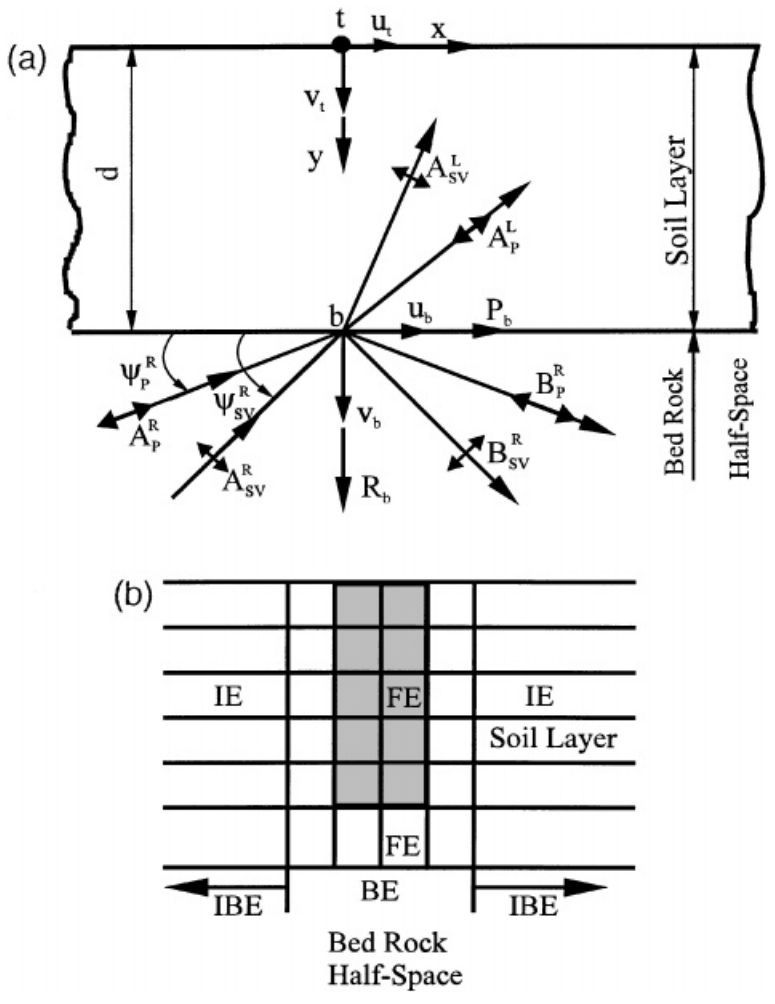

Figure 6. Numerical verification of free field response of soil layer and underlying half-space: (a) soil layer under wave incidence; (b) discretization of the soil layer

The soil medium is divided into six layers as shown in Figure 6(b). 24 four-node finite elements and 12 infinite elements are used for discretization of the layers, while the bed rock half-space is discretized into 4 BEs and 2 IBEs. The region of FEs with shadow in Figure 6(b) is selected for the solution domain of the near-field soil, while the surrounding ring of FEs is the transition zone for better connection with the far-field layers of IEs and the BE–IBE half-space. The comparison of magnification factors of the responses between the present results and the analytical solutions given by Wolf[17] is shown in Figures 7 and 8. The agreement between the two methods is excellent. Thus, the high accuracy of the presented model is verified.

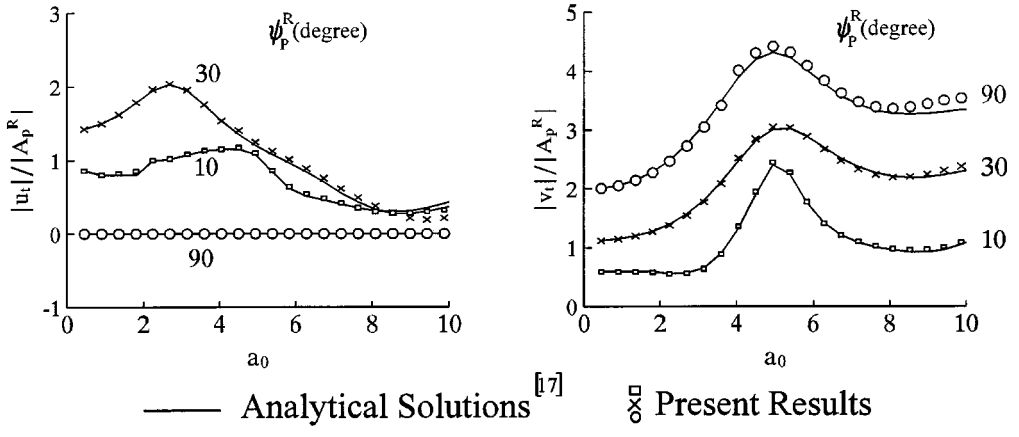

Figure 7. Comparison of free-field response of soil layer under *P* wave incidence

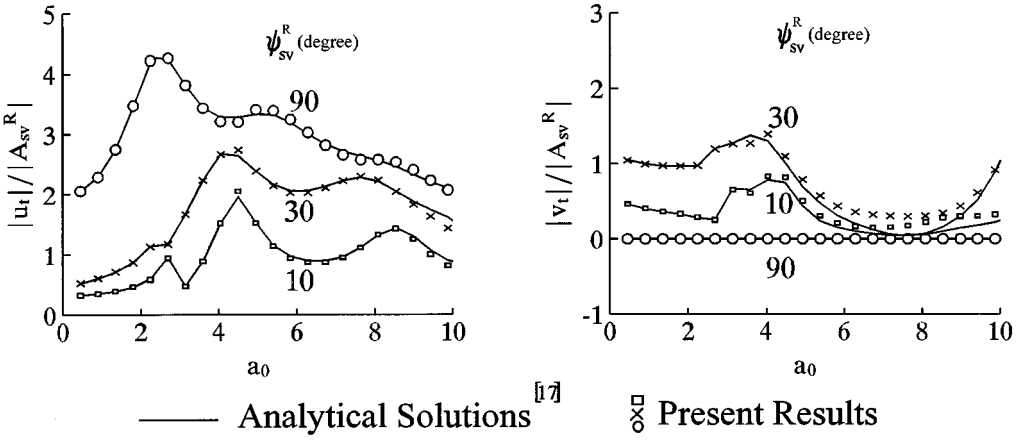

Figure 8. Comparison of free-field response of soil layer under SV wave incidence

3.2. The response of a soil–structure interaction system

Shown in Figure 9 is a typical test example of soil–structure interaction system given in Reference 2. Lysmer *et al.* studied this example for verification of the computer program FLUSH. Herein, the structure is modelled as beam elements and the embedded foundation of concrete is simulated as solid finite elements. The soil profile is assumed to have eight layers of which the first two are clay and the rest are sand. The soil layers within the dash line region denoted by elements A_i and D_i $(i = 1, 2, \ldots, 7)$ are selected as the near field of equivalent linear soil region. As mentioned previously, two stages of iteration need to be set up. After a preliminary convergence of the iteration obtained, the modulus and damping ratios of the transition and infinite elements B_i, C_i and E_i, F_i are changed to be the same as that of elements A_i and D_i, respectively.

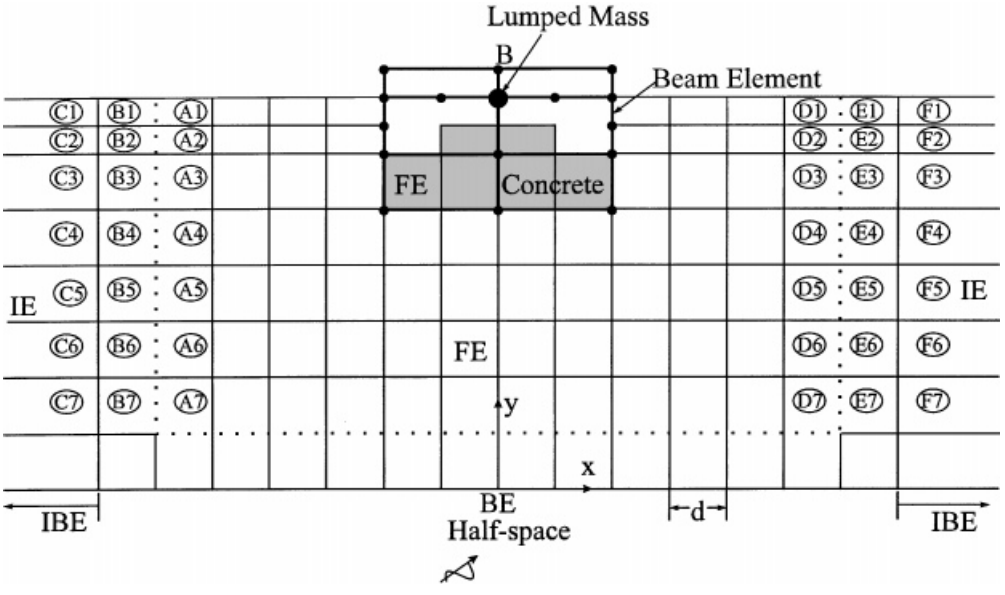

Figure 9. Soil–structure interaction system

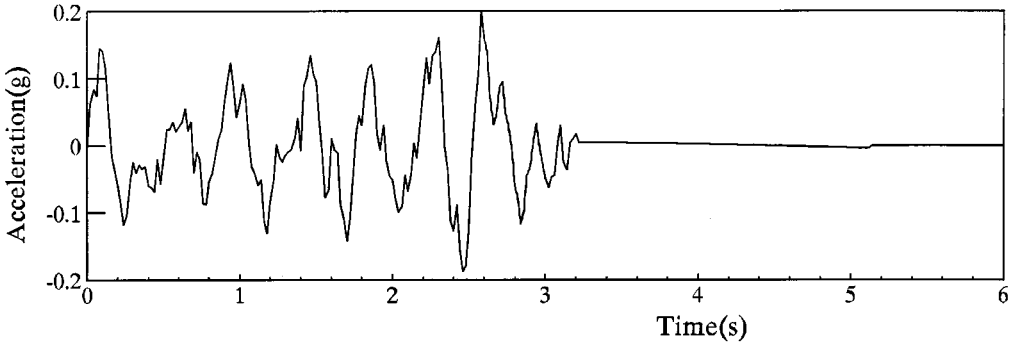

Figure 10. Earthquake time history as SV wave input

Then, additional iterations are needed for final convergence. This technique ensures the compatibility of parameters at the far field with that of the equivalent linear region while keeping the computation price at a reasonable level.

The typical normalized modulus and damping ratios versus shear strains provided by Seed[18] are used in the analysis.

In order to compare the present results with that obtained by FLUSH, a high value of modulus as 10^4 times as that of the neighbouring soil layer is assumed for the bed rock half-space. This high value of stiffness is equivalent to the rigid boundary assumption restricted in FLUSH. The horizontal ground motion with a maximum acceleration of 0·2 g shown in Figure 10 is assumed

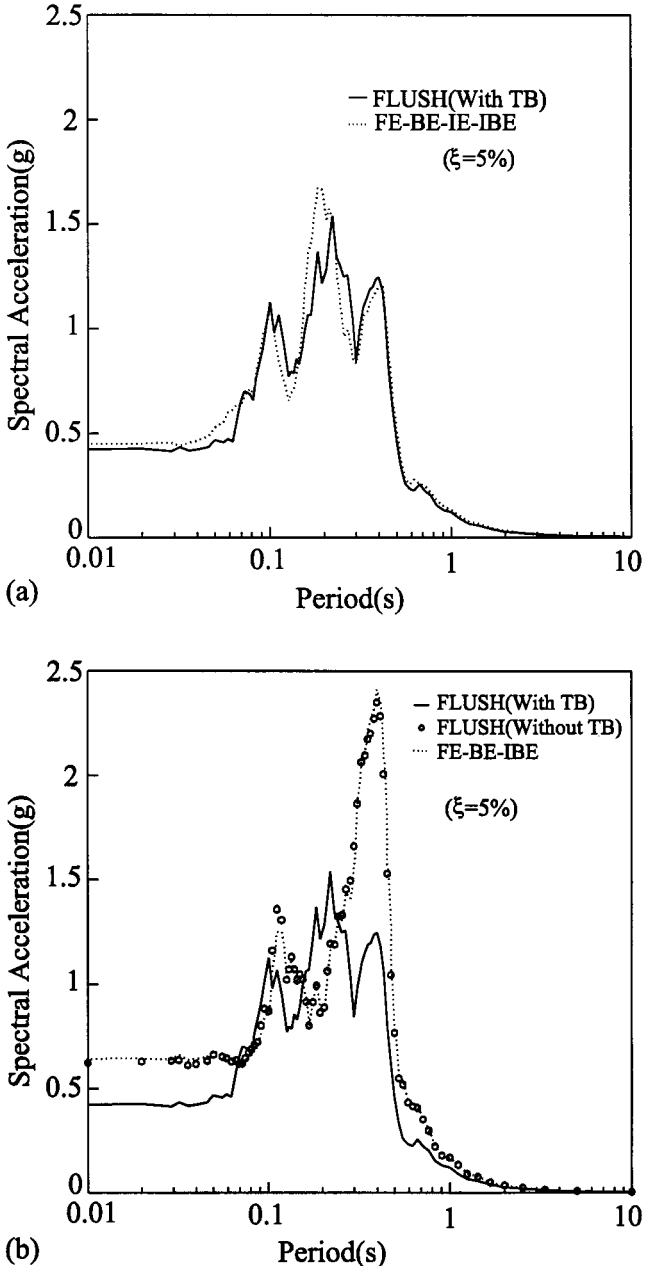

Figure 11. Comparison of response spectra at the top of structure with results by FLUSH program

to be acting at the rigid boundary for FLUSH. For present analysis, one-half of the above ground motion history is assumed as SV waves travelling from the bed rock. Thus, the earthquake input are approximately equivalent for the two methods. From Figures 11 and 12 the agreement

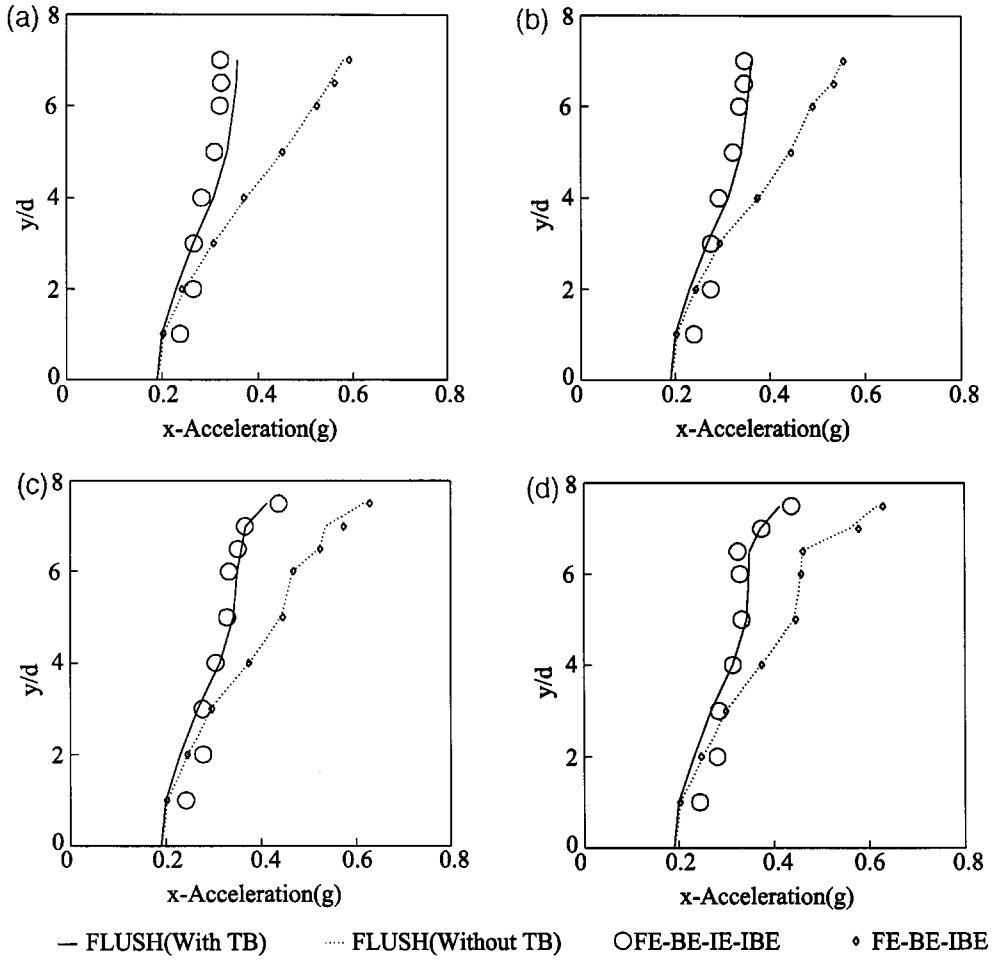

Figure 12. Comparison of response at different sections with results by FLUSH program with $|x|/d =$: (a) 5·0; (b) 3·0; (c) 2·0 and (d) 0·0

between current results and that given by FLUSH program is seen to be satisfactory. To demonstrate the effects of far field on the response, a study of boundary truncation by eliminating the IEs for the present model or the Transmitting Boundaries (TBs) for FLUSH. It is evident that the truncation of boundaries gives a significantly larger response than the results of considering the far-field effects. It can be concluded that the radiation damping is an important factor affecting the responses.

3.3. Effects of bed rock stiffness and non-vertical wave input

In order to examine the effects of the rock stiffness on the response of the structure and the soil, a series of different ratios of bed rock modulus are assume, i.e. $(E_r/E_s) = 1, 2, 4, 6, 9$, where E_r and

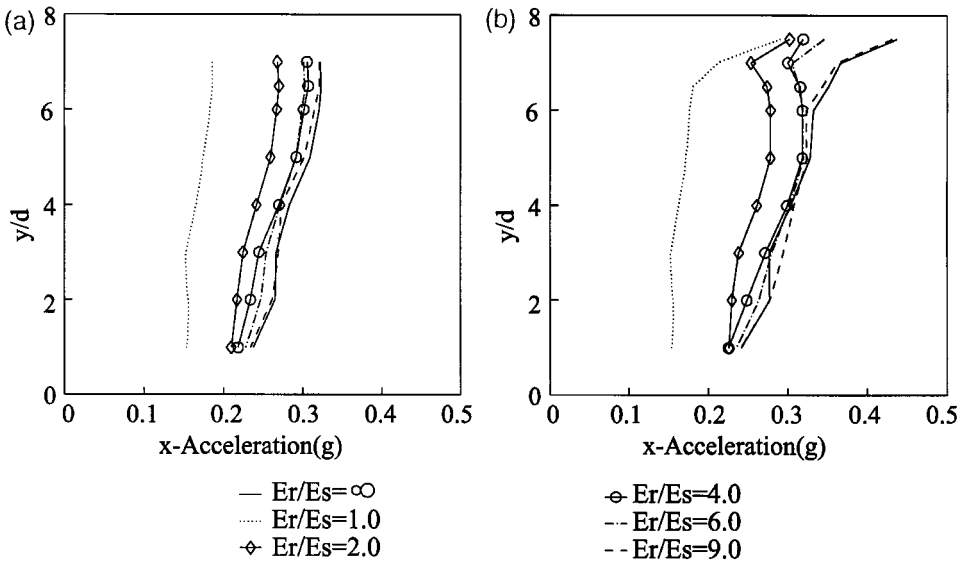

Figure 13. Effects of modulus ratio E_r/E_s on the soil structure response under SV wave input, with $x/d =$:(a) 5·0; and (b) 2·0

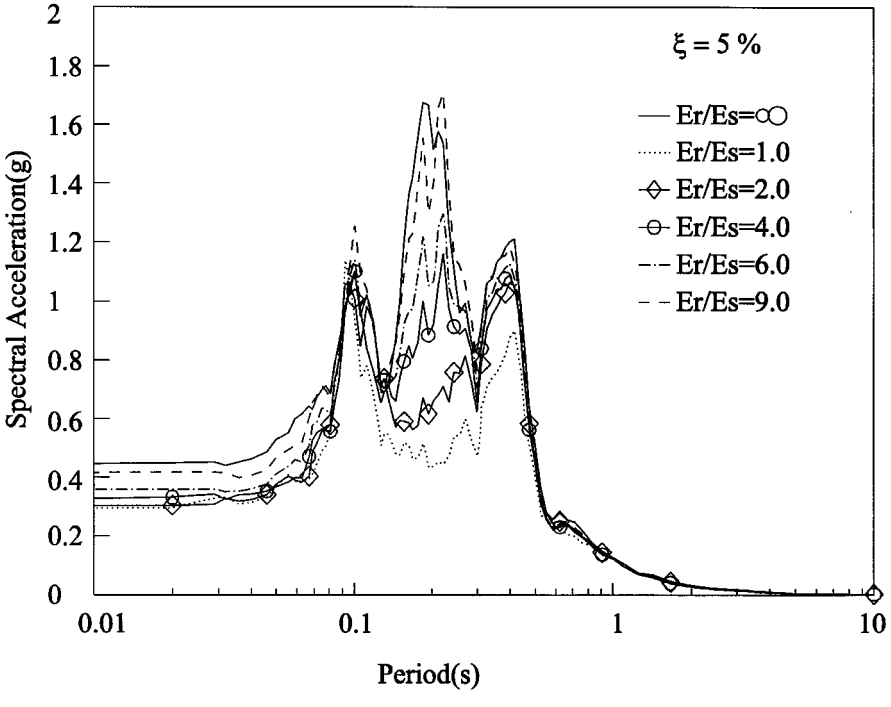

Figure 14. Effects of modulus ratio E_r/E_s on response spectra at top of the structure under SV wave input

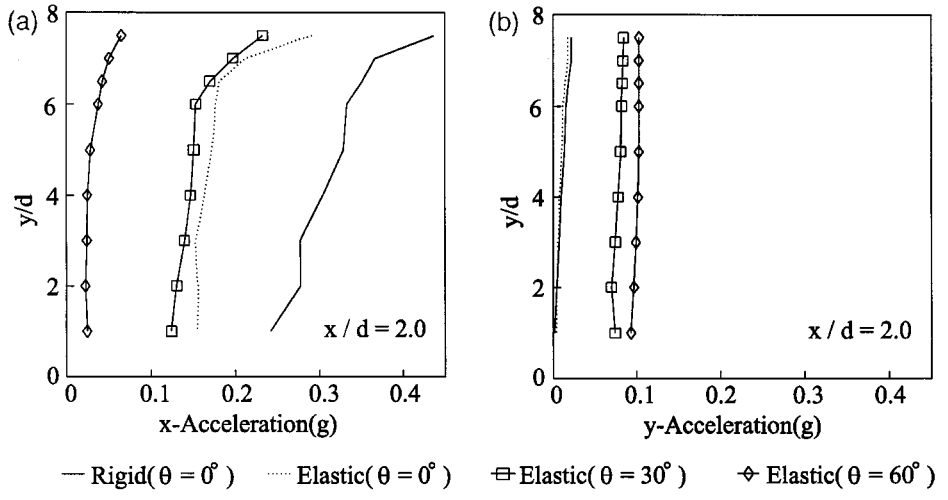

Figure 15. Effects of incident angles of SV waves on soil–structure response

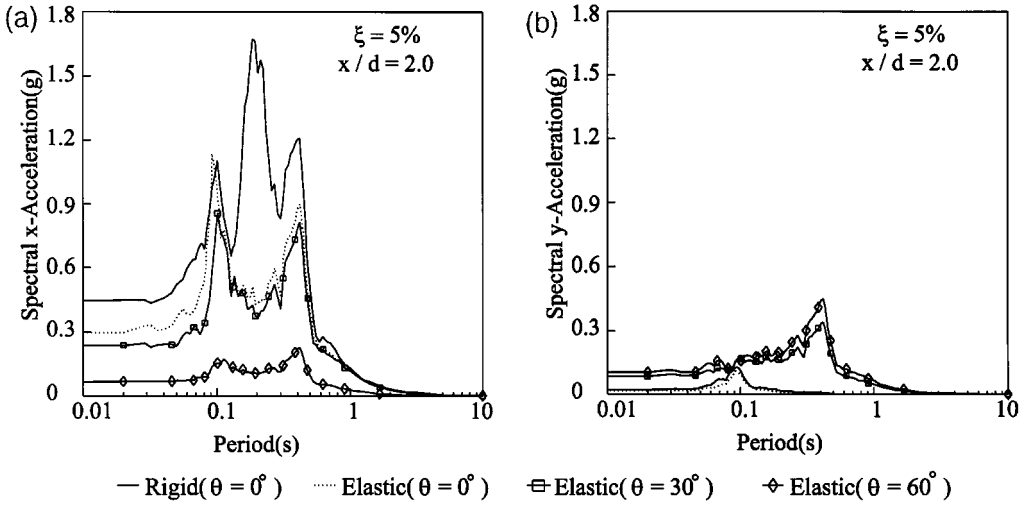

Figure 16. Effects of incident angles of SV waves on response spectra at top of the structure: (a) x-direction; (b) y-direction

E_s are modulus of the bed rock and the neighbouring soil layer, respectively. Figures 13 and 14 show the acceleration distribution along the depth of the soil and the response spectra at the top of the structure.

The results with $(E_r/E_s) = 10^4$ as a rigid boundary are also included in the figures for comparison. It appears that the response increases with the increase of rigidity of the bed rock. The most significant difference is seen at the bottom of the layers between the case of $(E_r/E_s) = 1{\cdot}0$ and the other ratios. This fact indicates the effects of wave amplification are significant at the

interface between the bed rock and the soil layers. For the current example the ratio of $(E_r/E_s) = 9{\cdot}0$ can be viewed as a rigid base condition.

Further study is to examine the influences of non-vertical wave input on the response. SV waves with different incident angles: i.e. $\theta = 0, 30, 60^\circ$ are assumed as the input. $(E_r/E_s) = 1{\cdot}0$ is assumed in this example. The results are shown in Figures 15 and 16. Observations arising from the results are summarized as follows: (1) When SV wave incidence is vertical (i.e. $\theta = 0^\circ$) the dominant responses in the soil and the structure are in horizontal, and vertical responses are insignificant. (2) When SV wave incidence is non-vertical, both horizontal and vertical responses are important. For example, when $\theta = 30^\circ$, the horizontal responses are smaller than the case of $\theta = 0^\circ$, but the vertical responses become more significant. In addition, the rocking motion produced from the phase difference due to inclined wave incidence may also become significant. Therefore, the resultant effects of non-vertical wave input may or may not increase in foundation motion and structural response depending on specific soil conditions and characteristics of the input waves. It is suggested that the input waves with different incident angles be considered for obtaining the critical response in the analysis.

4. CONCLUSIONS

In aseismic design and analysis of nuclear structures founded on sites of layered soil deposit, it is necessary to consider the following aspects in SSI analysis: (1) infinite and layer characteristics of the soil; (2) non-linear behaviours of the soft soil; (3) different input mechanism of earthquake waves from the bed rock. The objective of this study is to develop a coupling method of FE–BE–IE–IBE to satisfy the above requirements in an approximate manner. Based on the previous research on IEs and IBEs some improvements on these special elements are made for purpose of intercoupling. This includes developments of a four-node IE capable of transporting multi-waves and a type of IBE with traction attenuation. The FE–IE coupling is then used for simulation of infinite layered soil, and BE–IBE coupling is used to discretize the bed rock half-space. Thus, a complete model of structure–soil–bed rock system can be constructed.

With regard to the non-linearity of soil, the equivalent linear approach is employed allowing the system to be solved in the frequency domain. A substructuring technique is also adopted to restrict the solution domain to the near-field soil and the computational efforts can be reduced. The applicability and the accuracy of the method have been verified by comparing the present results of a test example with that given by FLUSH program. Studies on the effects of relative stiffness of the bed rock half-space and of different incident earthquake waves are also conducted. This method is now being employed for analysis of a nuclear plant built on deep soft soil.

ACKNOWLEDGEMENTS

The authors gratefully acknowledged the financial support for this work, which was provided by the Chinese National Key Projects on Basic Research and Applied Research (B). Appreciation is also expressed to Dr. Jin Feng for discussions.

REFERENCES

1. H. B. Seed and I. M. Idriss, 'Influence of soil conditions on ground motions during earthquake', *J. Soil Mech. Found. Div. ASCE* **95**, 99–137 (1969).

2. J. Lysmer, T. Udaka, C. F. Tsai and H. B. Seed, 'FLUSH–A computer program for approximate 3-D analysis of soil–structure interaction problems', *Report No. EERC 75-30*, Earthquake Engineering Research Center, University of California, Berkeley, CA, 1975.
3. J. Lysmer, Tabatabaie-Raissi, F. Tajirian, S. Vahdani and F. Ostadan, 'SASSI-A system for analysis of soil–structures interaction', *Report No. UCB/GT/81-02*, Earthquake Engineering Research Center, University of California, Berkeley, CA, 1981.
4. ASCE Standard: *Seismic Analysis of Safety-related Nuclear Structures and Commentary on Standard for Seismic Analysis of Safety Related Nuclear Structures*, ASCE, New York, ISBN 0-87262-582-6, September, 1986.
5. F. J. Rizzo, D. J. Shippy and M. Rezayat, 'A boundary integral equation method for radiation and scattering of elastic waves in three dimensions', *Int. J. Numer. Meth. Engng.* **21**, 115–129 (1985).
6. Zhang Chuhan and Song Chongmin, 'Boundary element technique in infinite and semi-infinite plane domain', *Proc. Int. Conf. BEM*, Pergamon Press, Oxford, 1986, pp. 551–558.
7. Zhang Chuhan, Song Chongmin and O. A. Pekau, 'Infinite boundary elements for dynamic problems of 3-D half-space', *Int. J. Numer. Meth. Engng.* **31** (1991) 447–462.
8. Zhang Chuhan, Jing Feng and O. A. Pekau, 'Time domain procedure for FE–BE–IBE coupling for seismic interaction of arch dams and canyons', *Earth. Engng. Struct. Dyn.* **24** (1995) 1651–1666.
9. R. F. Ungless, 'An infinite finite element', *MASc Thesis*, University of British Columbia, 1973.
10. P. Bettess, 'Infinite element', *Int. J. Numer. Meth. Engng.* **11** (1977) 53–64.
11. S. S. Saini, P. Bettess and O. C. Zienkiewicz, 'Coupled hydro-dynamic response of concrete gravity dams using finite and infinite elements', *Earth. Engng. Struct. Dyn.* **6** (1978) 363–374.
12. Y. K. Chow and I. M. Smith, 'Static and periodic infinite solid elements', *Int. J. Numer. Meth. Engng.* **17** (1981) 503–526.
13. F. Medina and J. Penzien, 'Infinite elements for elastodynamics', *Earth. Engng. Struct. Dyn.* **10** (1982) 699–709.
14. Zhang Chuhan and Zhao Chongbin, 'Coupling method of finite and infinite elements for strip foundation wave problems', *Earth. Engng. Struct. Dyn.* **15** (1987) 839–851.
15. Zhao Chongbin, Zhang Chuhan and Zhang Guangdou, 'Analysis of 3-D foundation wave problem by mapped dynamic infinite elements', *Sci. China* **32** (4) (1989) 479–491.
16. Zhang Chuhan and Wang Guanglun, 'Numerical model of the infinite domain and infinite elements', *Proc. 1st National Conf. on Combination Method of Analytical and Numerical Solutions*, Hunan University Press, 1990, pp. 6–44, ISBN 7-314-00492-7/N.11.
17. J. P. Wolf, *Dynamic Soil–Structure Interaction*, Prentice-Hall, Englewood Cliffs, NJ, 1985.
18. H. B. Seed and I. M. Idriss, 'Soil moduli and damping factors for dynamic response analysis', *Report No. EERC 70-10*, Earthquake Engineering Research Center, University of California, Berkeley, CA, 1970.

